Available online at www.CivileJournal.org

Civil Engineering Journal

(E-ISSN: 2476-3055; ISSN: 2676-6957)

Vol. 11, No. 07, July, 2025

Assessing Sediment Transport and Shoreline Dynamics in High-Energy Tropical Coasts

Hasdinar Umar [1*], Chairul Paotonan [1], Taufiqur Rachman [1], Sitti Hijraini Nur [2], Amir H. Muhiddin [3], Muhammad Idhil Maming [4], Andi M. Rezky Andriadi [4], Fuad Mahfud Assidiq [1]

[1] *Department of Ocean Engineering, Universitas Hasanuddin, Gowa, 92171, Indonesia.*

[2] *Department of Civil Engineering, Universitas Hasanuddin, Gowa, 92171, Indonesia.*

[3] *Department of Marine Science, Universitas Hasanuddin, Makassar, 90245, Indonesia.*

[4] *Department of Civil Engineering, Universitas Negeri Makassar, Makassar, 90224, Indonesia.*

Received 20 December 2024; Revised 07 June 2025; Accepted 12 June 2025; Published 01 July 2025

Abstract

This research examines coastal erosion in North Galesong, Indonesia, by validating longshore sediment transport (LST) equations and predicting shoreline changes over ten years. To evaluate sediment movement and coastline alterations, it integrates field data on sediment grain size and wave characteristics with numerical modeling techniques, including the CERC equation and finite difference methods. Sieve analysis revealed a range of sediment textures (D50: 0.17–0.65 mm), predominantly medium-fine sand. Wave analysis indicated a dominance of moderate energy southwesterly waves (1.5 m height, 6.39 s period) that aid sediment transport. The empirical LST models, calibrated with local data, closely matched numerical simulations (error <20%), predicting an annual net northward sediment transport of 406,869 m³. Shoreline analysis across 15 segments showed significant spatial variability: severe erosion occurred in Cell 4 (Δy = -0.82 m), while Cell 3 saw accretion (Δy = +0.68 m), influenced by wave direction, sediment supply, and coastal morphology. This study underscores the value of hybrid empirical-numerical methods in data-scarce regions and emphasizes the need for local model calibration to enhance coastal resilience. The findings inform sustainable management practices, promoting adaptive strategies to address sediment imbalances and hydrodynamic changes due to climate factors.

Keywords: Coastal Dynamics; Empirical Models; Longshore Sediment Transport; Shoreline Changes; Tropical Coastal Systems.

1. Introduction

Indonesia, the world's largest archipelagic nation, consists of approximately 17,000 islands and has the second-largest coastline in the world [1, 2]. This extensive area presents significant challenges in managing its dynamic coastal systems. Coastal zones, which act as the boundary between land and sea ecosystems, are inherently unstable due to wave action, tidal changes, and sediment movement. Longshore sediment transport (LST) plays a crucial role in shaping shorelines, leading to erosion or accretion [3, 4]. Erosion, characterized by shoreline retreat, threatens coastal infrastructure, ecosystems, and local livelihoods, while accretion involves sediment buildup that extends the shoreline. In the North Galesong District of Takalar Regency, coastal communities such as Tamasaju, Tamalate, and Aeng Batu-Batu experience notable erosion issues annually [5].

* Corresponding author: hasdinar.umar@gmail.com; hasdinarumar@unhas.ac.id

http://dx.doi.org/10.28991/CEJ-2025-011-07-022

Oceanographic factors, particularly wave energy [6] and longshore currents [7], significantly influence sediment transport along North Galesong's coast. Longshore currents, created by waves striking the shore at an angle, transport sediments parallel to the coastline, affecting erosion and accretion patterns. However, the reliability of empirical models for predicting these changes in high-energy tropical regions like Sulawesi is still largely unexamined. While the CERC formula [8] and Komar's equations [9] are commonly used to estimate longshore transport (LST), their effectiveness in data-scarce areas such as North Galesong—marked by diverse sediment grain sizes, varying wave conditions, and human activities like sand mining—has not been thoroughly assessed. This lack of evaluation complicates coastal management, as choosing the right model is crucial for accurately predicting shoreline changes.

Recent studies on Sulawesi's coastlines highlight erosion, exacerbated by natural and human factors. Pananrangi [10] identified land subsidence and sand extraction as key causes of erosion in Galesong. Prasetyo et al. [11] noted significant coastal degradation in North Galesong due to increased wave energy and sediment scarcity. These findings align with broader regional trends, as coastal areas in Western and Eastern South Sulawesi, including Pare-pare City and Pinrang Regency, are particularly vulnerable to erosion from variable wave conditions and human activities like coastal development [12]. Similarly, Amurang in North Sulawesi has seen coastline changes with an annual erosion rate of 1.05 hectares, mainly due to tidal forces and land reclamation disrupting sediment balance [13]. Current research primarily relies on qualitative risk assessments or singular analytical methods, such as the Equi-Wave Phase Potential (EWPP) model, which measures erosion from sand mining but overlooks broader ecological interactions [14]. In contrast, the Coastal Vulnerability Index (CVI) employs multi-parameter frameworks, including land cover and shoreline erosion rates, to evaluate vulnerabilities comprehensively, aiding in developing targeted management strategies [15]. Semi-quantitative methods, like traffic-light mapping systems, underscore hazard and vulnerability indices, highlighting the role of cultural ecology in enhancing resilience [16]. However, the diverse methodologies, from grid-based coastal risk models [17] to multi-index erosion assessments, expose a critical gap: the lack of comparative analyses to determine which empirical models best capture the varied coastal dynamics of Sulawesi. This deficiency impedes the development of adaptive mitigation strategies, as evidenced in Maros, where both structural (e.g., breakwaters) and nonstructural (e.g., community empowerment) efforts are constrained by poor regulatory enforcement and data integration [18]. Without systematic evaluations of model performance across Sulawesi's diverse coastal settings, effective erosion countermeasures will remain insufficient, continuing to threaten ecosystems and vulnerable communities.

Over the decades, global empirical formulas for predicting land surface temperature (LST) and shoreline changes have evolved. The CERC equation [8], linking wave energy and breaker angle to sediment transport rates, is widely accepted for its simplicity and validation. Komar's method [9] improves upon this by incorporating sediment grain size and wave period, offering a more nuanced analysis for diverse coastal settings. However, regional studies in tropical areas reveal that these models' accuracy declines when applied beyond their original calibration. This underscores the need for localized validation, particularly in Sulawesi, where high-energy swells [19, 20] and monsoonal winds [21] are significant factors. Moreover, previous literature studies have mainly concentrated on risk indices without adequately addressing sediment transport processes, and local government reports often lack methodological rigor. This research seeks to address these gaps by evaluating various empirical models to determine their effectiveness in predicting shoreline changes in North Galesong. By integrating field-collected sediment grain size data, wave predictions, and hydrodynamic factors, this study provides the first comprehensive assessment of empirical methods in Sulawesi's high-energy coastal environment. This study is original in two significant ways: (1) it validates empirical LST formulas using localized data, and (2) it forecasts shoreline changes over a decade to identify areas of erosion and accretion. This methodology enhances the understanding of sediment dynamics in tropical coastal regions and supports evidence-based coastal protection policies.

The study is organized as follows: Section 2 outlines the methodology, including data collection, wave forecasting, sediment transport calculations, and shoreline change modeling. Section 3 presents results on sediment characteristics, wave climate, LST rates, and predictions of shoreline evolution based on empirical methods. Section 4 discusses the implications for coastal management, emphasizing the strengths and limitations of the methodology. Finally, Section 5 concludes by summarizing key findings and suggesting future research directions.

2. Method

2.1. Research Flow Framework

The methodological framework illustrated in Figure 1 employs a systematic strategy to examine coastal sediment dynamics and shoreline changes, merging empirical research with field and secondary data sources. The investigation commences with a comprehensive literature review to contextualize regional coastal processes and establish foundational parameters for sediment transport and wave modeling. Primary data collection involves sediment sampling and wind measurements, while secondary data encompasses historical shoreline positions obtained from Google Earth imagery and sediment distribution patterns analyzed through sieve techniques. Granulometric testing of sediment samples is conducted to ascertain grain size distributions, subsequently guiding the selection of empirical formulas for calculating longshore sediment transport. Wave forecasting, informed by wind data and wave rose analysis, supplies essential inputs for modeling hydrodynamic conditions, including breaking wave characteristics that affect sediment mobilization. The CERC [8] empirical formula is utilized to quantify longshore sediment transport rates, which are spatially distributed across coastal cells to assess sediment budget gradients. The analysis of shoreline changes employs

numerical equations derived from sediment transport rates and specific morphological parameters for each cell, with results visualized through geospatial mapping (WGS 1984 UTM Zone 51S) to evaluate erosion and accretion trends. This integrated framework establishes a strong connection between sedimentological, hydrodynamic, and geospatial datasets, facilitating identifying key processes that influence coastline evolution.

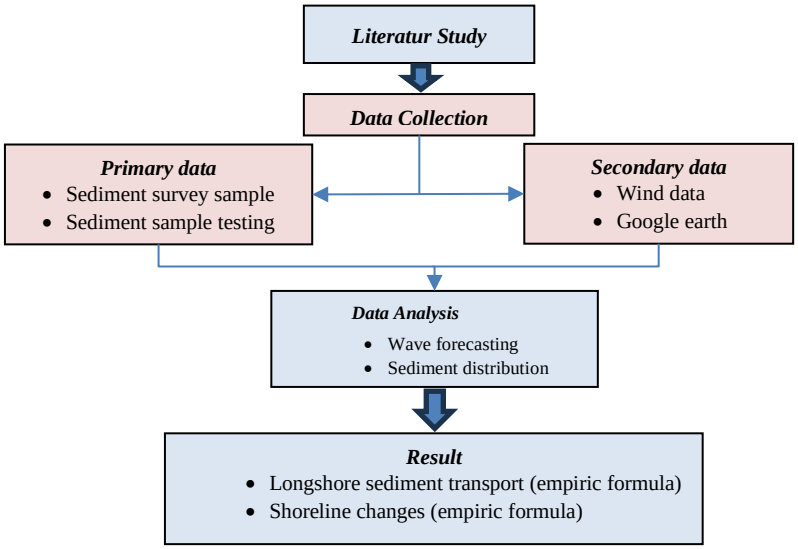

Figure 1. Flowchart of the research methodology

2.2. Research Location

This research was carried out at three beach locations in South Sulawesi: Aeng Batu-Batu Village Beach, Tamalate Village Beach, Tamasaju Village Beach, North Galesong District, Takalar Regency. Takalar Regency is one of the regencies located in South Sulawesi Province. The capital of Takalar Regency is situated in Pattalassang. The area of Takalar is 566.51 km2, with a population of 304,856 people [22]. Administratively, this regency consists of 76 villages and 24 sub-districts located in 10 sub-districts, namely Mangarabombang, Mappakasunggu, Sanrobone, South Polombangkeng, Pattalassang, North Polombangkeng, South Galesong, Galesong, North Galesong and Tanakaeke Islands. Based on its geographical position, Takalar Regency has boundaries: to the east, it borders the Gowa and Jeneponto Regencies. To the north, it borders Gowa Regency, while to the west and south, it is bordered by the Makassar Strait and the Flores Sea (Figure 2).

Galesong District has abrasion problems along its coastline. This abrasion continues until it erodes public facilities and people's homes. This is caused by high wave energy and exacerbated by sand mining activities at sea [10]. One of the areas in Takalar Regency that is vulnerable to abrasion is the coast of North Galesong. According to the strategic issues of the Takalar Regency RTRW 2010–2030, the coast of North Galesong District, which faces the Makassar Strait, is an area that often experiences abrasion disasters every year. The result is damage to productive agricultural land and the road network. Natural factors, such as high coastal currents, tides, waves, and strong winds, can cause abrasion [11].

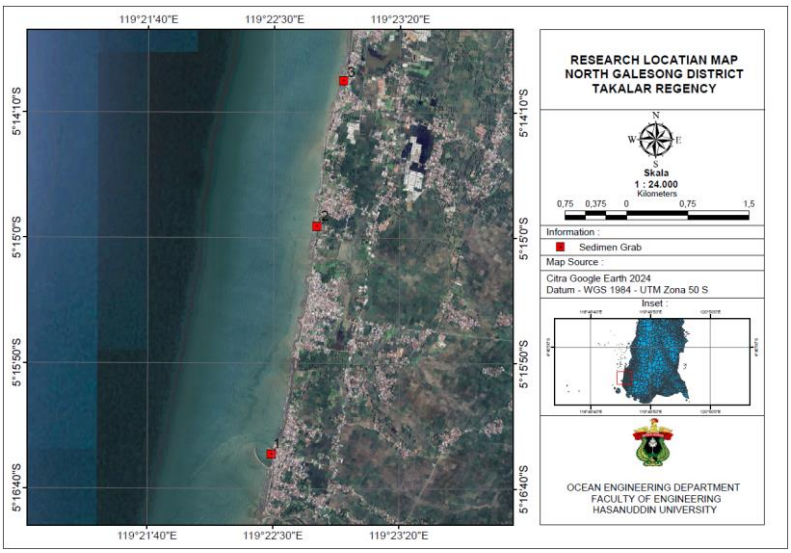

Figure 2 Research Location

2.3. Wind Analysis

The Sultan Hasanuddin Meteorological Station wind data was obtained online and processed using WRPlot View. The classification of the data obtained is the maximum daily wind speed and direction; the data used is the result of station observations for the last ten years, starting from 2014 to 2024. The analysis results are displayed in Windrose form below.

Based on Figure 3, the dominant maximum wind direction comes from the west, with the most significant percentage of occurrences. The study location is on the western side of the mainland, so based on the location of the study location, a relatively western wind direction is used.

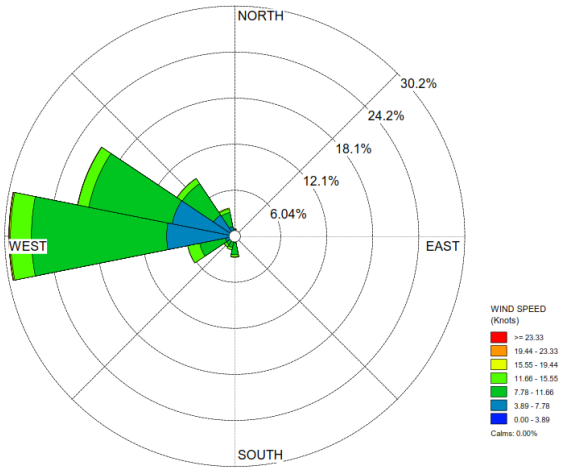

Figure 3. Wind Rose

2.4. Fetch Analysis

Adequate fetch data at the study location must be known to predict the wave. In reviewing wave generation, land is categorized as a boundary in fetch calculations. In the wave formation area, it is assumed that the waves do not move in a constant direction along the wind but at various angles to the direction of the wind movement. The fetch is determined by the direction that can produce waves. The fetch is done with the help of ArcGIS and MS software (Excel). The fetch length is generally limited based on the shape of the land surrounding the wave-generating area and is measured based on the direction of the wind gusts (Figure 3). The following formula calculates the average effective fetch [23].

$$F_{eff} = \frac{\Sigma X_i \cos a}{\Sigma \cos a} \quad (1)$$

With F_{eff} is effective average fetch, X_i is number of fetch measurements, and a is fetch measurement angle. Based on analysis at the study location, the effective fetch length was 410.13 km

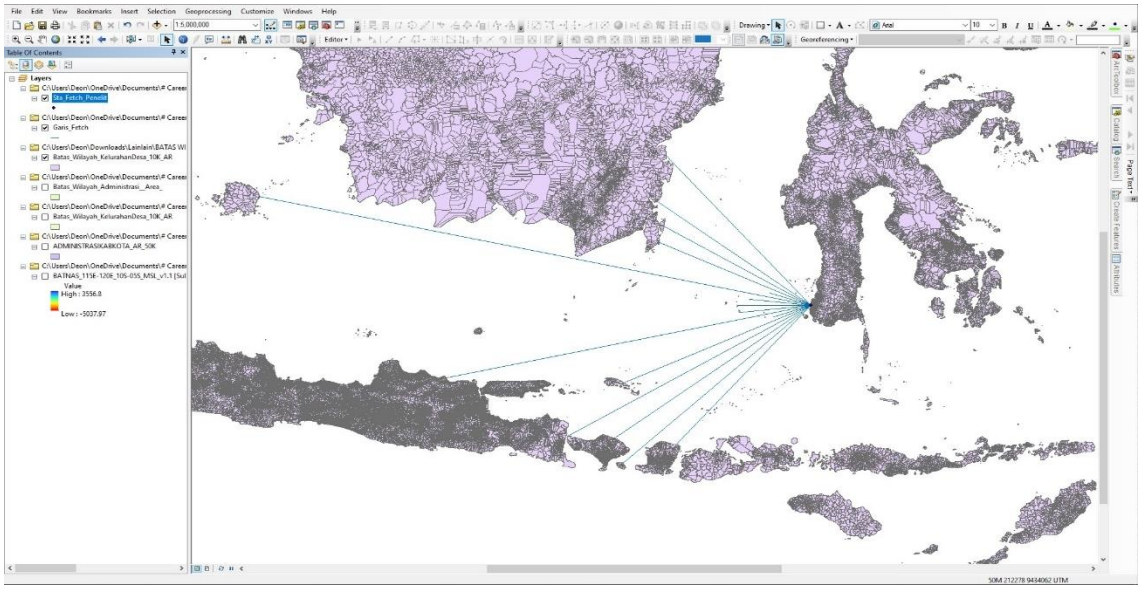

Figure 4. Practical fetch analysis at the Study location

2.5. Wave Forecasting

Effective wind and fetch data are needed to predict wave height in the deep sea. The wind data obtained previously was corrected into a wind stress factor before analyzing wave height in the deep sea (Figure 5). From the conversion results, an analysis of wave forecasting in the deep sea is then carried out using the fetch-limited formula and the help of wave forecasting charts. The following are the wave height measurements obtained and presented as wave roses.

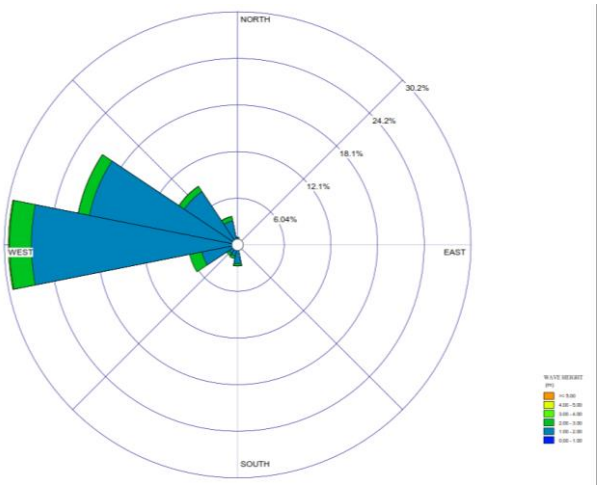

Figure 5. Wave Rose at Research Location

2.6. Sediment Analysis

The sampling locations were Aeng Batu-Batu Village Beach, Tamalate Village Beach, and Tamasaju Village Beach, North Galesong. Sampling at 15 locations was taken. The tool used to determine the location of the coordinates of each point is GPS (Global Position System). The coordinates of the points can be seen in Table 1. Moreover, the position of each sediment sampling point can be seen in Figures 6 and 7.

Table 1. Coordinates of Beach Sediment Sampling Points

Number	Point	Marked	Coordinates	
			Latitude	Longitude
1	TK 1		5°13'3.12"	119°22'59.68"
2	TK 2		5°13'26.32"	119°22'59.73"
3	TK 3		5°13'49.1"	119°22'57.76"
4	TK 4		5°14'1.94"	119°22'54.76"
5	TK 5		5°14'15.36"	119°22'50.51"
6	TK 6		5°14'26.01"	119°22'48.84"
7	TK 7		5°14'34.34"	119°22'48.09"
8	TK 8		5°14'39.48"	119°22'47.75"
9	TK 9		5°14'47.46"	119°22'46.9"
10	TK 10		5°14'54.68"	119°22'46.13"
11	TK 11		5°14'16.04"	119°22'43.13"
12	TK 12		5°14'32.03"	119°22'40.01"
13	TK 13		5°16'12.18"	119°22'33.6"
14	TK 14		5°16'31.36"	119°22'28.48"
15	TK 15		5°16'42.86"	119°22'26.37"

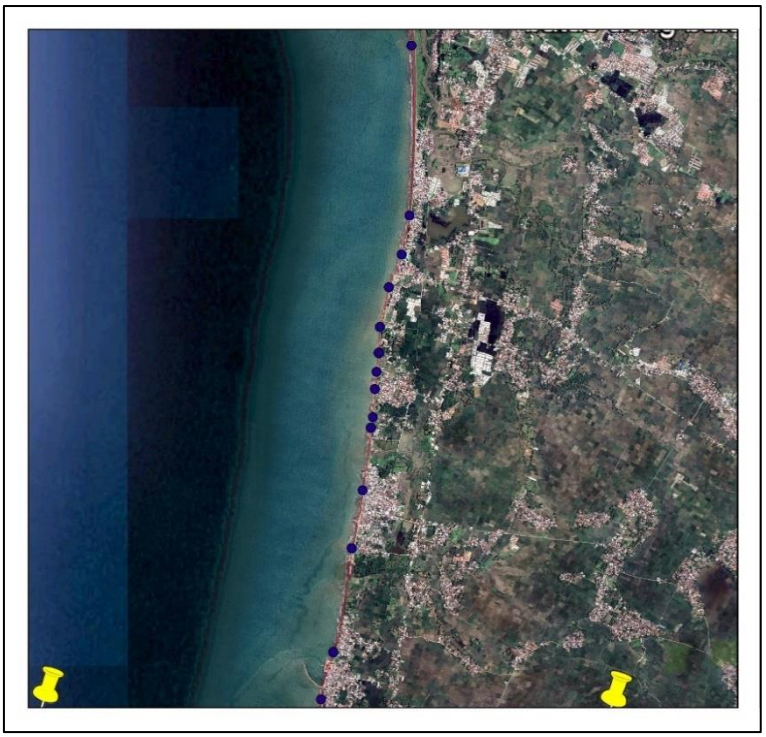

Figure 6. Map of Sediment Sampling Points

Figure 7. Sediment Sampling at Research Locations

2.7. Longshore Sediment Transport

Coastal sediment transport is the movement of sediment in coastal areas caused by waves and the currents they generate. Sediment transport is divided into 2 types, namely: transport to and from the coast (onshore-offshore transport) which has an average direction parallel to the coast. Sediment transport along the coast can be calculated using the following formula [8]:

$$Q_s = K.P_i^n \tag{2}$$

$$Q_s = p.A.H_o^2.C_o.(K_{rbr})^2.\sin\alpha_b.\cos\alpha_b \tag{3}$$

where Q_s is longshore sediment transport (m^3/year), p is percentage of wave occurrences in the direction and wave height under consideration, A is CERC coefficient = 0.61 × 106 sd 0.79 × 106 H_o is wave height depth sea (m), C_o is wave propagation (m/s), K_{rbr} is reflection coefficient, α_b is breaking wave angle.

2.8. Shoreline Changes

The coastline is the boundary between land and water that will change over time. The process of changing the coastline is caused by erosion (abrasion) and addition/accretion factors [24]. Changes in the coastline that occur in coastal areas are in the form of erosion of the coastal body (abrasion) and addition of the coastal body (sedimentation or accretion). These processes occur as a result of the movement of sediment, currents, and waves that interact directly with the coastal area [25].

The process of coastal change includes erosion and accretion processes. Erosion around the coast can occur if the transport of sediment that comes out or moves to leave an area is greater than the transport of sediment that enters; if the opposite occurs, then what happens is sedimentation [23].

The imaginary line where water and land meet is also called the coastline. As a result, the phenomena around the coast cause fluctuations relative to the coastline in terms of slope, rate of change, and form of change. Changes greatly influence lines that are pseudo-movement or imaginary in hydrogenotrophic factors [26]. The stages of the sedimentation process that lead to changes in the coastline are:

1. Stirring cohesive material from the bottom to suspension or releasing non-cohesive material from the seabed.
2. Cohesive material movement.
3. Re-deposition of the material.
4. Changes in the morphology of the line based on scale are:
    a. Short-scale coastal morphology changes (micro-scale)
    b. Longer-scale coastal morphology changes (meso scale); the coast experiences seasonal changes due to changes in the characteristics of the seasons that have an annual cycle.
    c. On a longer time and space scale (macro-scale), the coast can be said to experience erosion or accretion if the average coastline advances or retreats during that period.

Calculation of coastline changes using empirical methods [27]:

$$\Delta y = \frac{\Delta t}{d_b \times \Delta x}(Q_{i+1} - Q_i) \quad (4)$$

3. Results and Discussion

3.1. Sediment Characteristics

Sediment testing at the beaches of Aeng Batu-batu Village, Tamalate Village, and Tamasaju Village took the form of sieve analysis. According to ASTM (American Society for Testing and Materials), analysis of the grain size of this sediment was carried out in the Marine Engineering Department Laboratory, as presented in Figure 8. Sieve analysis was carried out using the sieve net sieve method with diameters of 4.75 mm, 0.85 mm, 0.425 mm, 0.3 mm, 0.25 mm, 0.15 mm, 0.075 mm and in dry conditions. The filters are arranged from top to bottom, with the arrangement going down the filter getting tighter and ending in the pan. Then, the dry sediment sample is poured onto the filter structure, covered, and placed on the sieve shaker to begin filtering until each sediment size fraction is separated for 15 minutes. After the sieve shaker stops, slowly lower the sieve assembly. Separate the filters one by one, weigh the sediment retained on each filter with a digital scale, and record the weight of the sediment retained on the form that has been prepared.

Figure 8. Sediment Sample Testing at the Coastal Geotechnical Laboratory of the Department of Coastal Engineering

A thorough screen analysis was performed on all sediment samples. For example, the sieve analysis results for the sample from point 1 are shown in Table 2. The sediment sample from point TK 1 (AENG1) underwent analysis using sieves with mesh sizes from 4.7 mm to 0.075 mm, plus a pan for the finest particles. The total sample mass was 771.2 grams. Coarser fractions were minimal, with only 0.285% retained on the 4.7 mm sieve, while finer sieves captured the majority. Specifically, the 0.425 mm sieve retained 24.326%, leading to a cumulative retention of 40.949% up to that size. Finer fractions were significant, with 18.996% on the 0.25 mm sieve and 17.038% on the 0.15 mm sieve, indicating a prevalence of medium- to fine-grained particles. The 0.075 mm sieve captured 13.939%, and the pan collected 0.195%. Cumulative retention in the pan reached 100%, with particles passing through decreasing from 99.715% at the 4.7 mm sieve to 0.000% in the pan. This data reflects a well-graded particle size distribution, with a notable concentration of finer fractions below 0.425 mm, underscoring the sediment's heterogeneity, particularly within the 0.15–0.425 mm range.

Table 2. Sediment Sample Filter Analysis Results

Point	Sieve Number	Diameter (mm)	Suspended Weight (grams)	Percent Retained (%)	Accumulative Hold (%)	Percent Passed (%)
TK 1 (AENG 1)	4	4.7	2.20	0.285	0.285	99.715
	16	0.85	126.00	16.338	16.623	83.377
	20	0.425	187.60	24.326	40.949	59.051
	40	0.3	68.50	8.882	49.831	50.169
	60	0.25	146.50	18.996	68.828	31.172
	100	0.15	131.40	17.038	85.866	14.134
	200	0.075	107.50	13.939	99.805	0.195
	Pan	Pan	1.50	0.195	100.000	0.000
Total Weight			**771.2**			

The sediment grain size distribution analysis for point TK 1 (AENG1) reveals a well-graded composition, illustrated in Figure 9, which shows a logarithmic distribution curve typical of fluvial or coastal sediments. The graph plots particle diameter (in mm) against the percentage of particles passing through, with the D50 value—representing the median grain size—identified at the intersection of the 50% passing line and the distribution curve, extending to the diameter axis. For this sample, the D50 was 0.32 mm, indicating a prevalence of medium- to fine-grained sediment. This aligns with sieve analysis results, which indicated significant concentrations in the 0.25–0.425 mm range, comprising 18.996% to 24.326% of the sample, while finer particles (under 0.15 mm) constituted 17.038% to 13.939% of the total weight. The log-linear pattern in the grain size distribution graph underscores the sediment's variability, reflecting diverse transport processes and depositional environments. The D50 value of 0.32 mm is crucial for understanding sediment texture and hydrodynamic conditions at this site, corroborating sieve analysis findings that show a gradual increase in fine-grained fractions as particle size decreases.

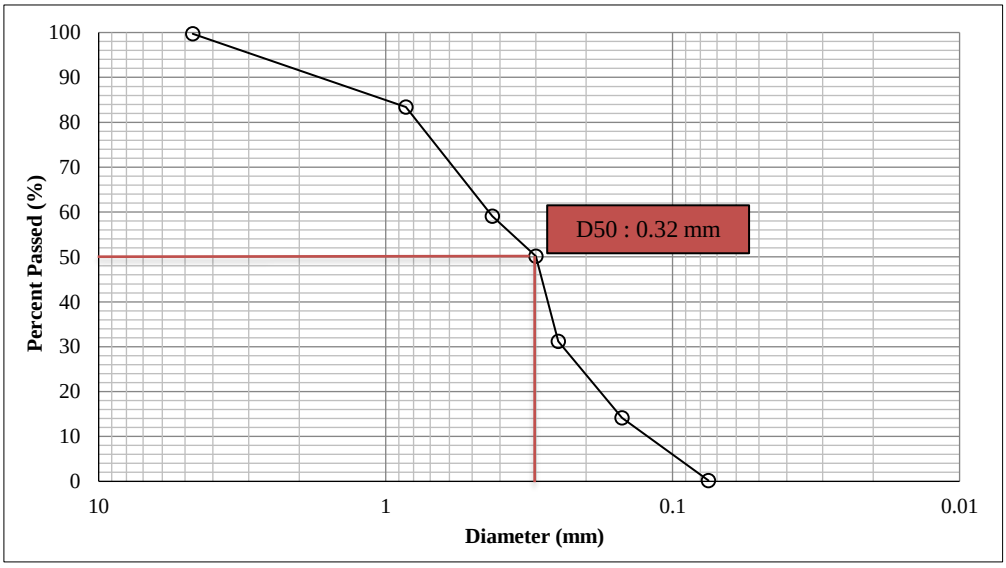

Figure 9. Sediment Grain Distribution Graph

The sediment grain size analysis across various sampling sites, Table 3, reveals a predominance of medium to fine sand textures along the beaches of Aeng Batu-Batu Village, Tamalate Village, and North Tamasaju Galesong Village, with D50 values between 0.17 mm and 0.65 mm. Many samples (e.g., IK1, IK2, IK3, TK7, TK9) exhibit D50 values from 0.22 mm to 0.29 mm, classifying them as fine to medium sand, while coarser samples (e.g., TK4 and TK15, with D50 values of 0.64–0.65 mm) are categorized as coarse sand. This aligns with the grain size distribution in Table 2 (AENG1), where 40.95% of sediment mass is retained in the 0.425 mm sieve, indicating a mixed sedimentary environment. The presence of medium sand (0.25–0.5 mm) at sites like IK5 (D50 = 0.43 mm) and IK14 (D50 = 0.48 mm) suggests moderate hydrodynamic conditions, while finer sediments (0.125–0.25 mm) at IK3 (D50 = 0.17 mm) and TK7 (D50 = 0.23 mm) may indicate lower energy environments or enhanced retention of fine particles. The absence of gravel-sized particles (>2 mm) and the limited presence of very coarse sand (>0.5 mm) suggest a lack of high-energy fluvial or wave-driven processes in these coastal regions. However, the spatial variability in grain size, particularly the coarser sediments at TK4 and TK15, may indicate localized influences from littoral drift, human activities, or variations in sediment supply, warranting further investigation into sediment transport dynamics and depositional factors. The consistency between sieve analysis (Table 2) and D50 classifications (Table 3) supports the reliability of these findings, which are crucial for understanding coastal morphodynamics and informing sustainable shoreline management practices in the region.

Table 3. Sediment Grain Diameter at Each Point

Sample	Diameter D_{50} (mm)	Specific Gravity
TK 1	0.32	Medium Sand
TK 2	0.22	Fine Sand
TK 3	0.17	Fine Sand
TK 4	0.65	Rough Sand
TK 5	0.43	Medium Sand
TK 6	0.30	Medium Sand
TK 7	0.23	Fine Sand
TK 8	0.24	Fine Sand
TK 9	0.25	Fine Sand
TK 10	0.28	Medium Sand
TK 11	0.27	Medium Sand
TK 12	0.29	Medium Sand
TK 13	0.26	Medium Sand
TK 14	0.48	Medium Sand
TK 15	0.64	Rough Sand

3.2. Longshore Sediment Transport

Sedimentation processes in the coastal regions of Aeng Batu-Batu, Tamalate, and North Tamasaju Galesong Villages are significantly influenced by wave characteristics, as shown in Table 4. Wave forecasting indicates a predominant pattern from the southwesterly to west-southwesterly direction, with a notable concentration of waves (up to 4.55%) in the 1.5 m height category (period: 6.39 s), particularly from the W-SW direction. Conversely, the occurrence of higher wave heights (2.5 to 4.5 m) is much lower (≤1.62%), indicating that extreme wave events are rare in this area. This suggests that sediment transport and deposition are primarily driven by moderate-energy wave conditions, which align with the fine to medium sand fractions (D50: 0.17–0.65 mm) found in sediment grain size analyses (Table 3). The dominance of lower wave energies likely promotes the accumulation of finer sediments, as coarser particles require higher energy for mobilization. However, the infrequency of significant wave activity exceeding 2.5 m raises questions about the influence of seasonal storms or human activities on sediment supply. The consistent W-SW wave direction may indicate a stable littoral drift system, impacting shoreline morphology and sediment sorting. Researchers can better understand spatial variations in depositional environments by correlating wave data with sediment grain size distributions (e.g., D50 values). However, it is crucial to consider factors like wave-breaking dynamics and sediment-specific transport rates.

Table 4. Direction and Percentage of Wave Occurrence

H_o (m)	T (s)	Direction and Percentage of Wave Occurrence		
		S – SW	SW	W-SW
0.5	3.96	0.03	0.03	0.14
1.5	6.39	1.45	1.31	4.55
2.5	7.45	0.36	0.36	1.62
3.5	8.30	0.00	0.00	0.00
4.5	9.51	0.00	0.00	0.00

The parameters of breaking waves in Table 5 offer critical insights into the hydrodynamics of nearshore environments. Wave heights (H) range from 0.5 m to 4.5 m, with periods (T) between 3.96 and 9.51 seconds. A correlation exists between increased wave height and greater wavelength (L) and wave celerity (Co), with L values from 24.43 m to 141.16 m and Co values from 6.17 m/s to 14.83 m, indicating deeper water conditions. The breaker height (H') and the ratio H'/Lo, which spans from 0.016 to 0.026, imply a shift from spilling to plunging breakers. The H/H_0 values, ranging from 1.15 to 1.30, reflect moderate energy dissipation during breaking. These parameters relate to sediment transport dynamics; notably, higher H'/Lo ratios (≥0.023) at 2.5 m to 4.5 m wave heights indicate increased turbulence that can mobilize coarser sediments. The rarity of extreme wave heights (≥3.5 m) aligns with the dominance of fine- to medium-grained sands (D50: 0.17–0.65 mm) in sediment studies, underscoring the connection between wave energy and coastal sediment characteristics.

Table 5. Breaking Wave Parameters

H_o (m)	T (s)	L_o (m)	C_o (m/s)	H'_o (m)	H'_o/L_o	H_b/H'_o	H_b (m)	H_b/gT^2	d_b/H_b	d_b
0.5	3.96	24.43	6.17	0.4	0.016	1.30	0.520	0.0034	1.21	0.6292
1.5	6.39	63.76	9.97	1.2	0.019	1.22	1.464	0.0037	1.21	1.7714
2.5	7.45	86.64	11.62	2	0.023	1.18	2.360	0.0043	1.22	2.8792
3.5	8.30	107.51	12.95	2.8	0.026	1.15	3.220	0.0048	1.22	3.9284
4.5	9.51	141.16	14.83	3.6	0.026	1.15	4.140	0.0047	1.22	5.0508

The combination of wave rose data, breaking wave parameter, and sediment grain size analysis using the CERC formula [8] facilitated a thorough evaluation of longshore sediment transport dynamics within the study region. Table 6 presents the directional sediment transport rates categorized by various wave height intervals and approach angles, highlighting specific trends in Cell 1. The southward transport, primarily influenced by S-SW, SW, and W-SW wave directions, represented substantial sediment volumes (for instance, 114,128 m³/year from W-SW waves at heights between 1.5 and 2.5 m), driven by moderate-energy wave conditions (H = 0.5–2.5 m) and significant occurrence rates (up to 4.55% for W-SW waves). In contrast, the northward transport, affected by W, W-NW, NW, and N-NW waves, demonstrated more excellent cumulative rates (for example, 294,334 m³/year from W-NW directions), especially under lower wave heights (0.5–2.5 m) and extended durations. Table 7 consolidates these findings, indicating a net northward sediment transport of 406,869 m³/year, surpassing the southward contributions of 211,279 m³/year. This difference underscores the predominance of northward littoral drift, likely influenced by wave angle asymmetry and sediment availability. The dominance of fine to medium-grained sands (D50: 0.17–0.65 mm) corresponds with transport capacity thresholds, as finer particles are more easily mobilized under moderate wave energies.

Table 6. Longshore Sediment Transport at Cell 1

Direction of Wave Incoming	Wave Data	H (m)	Angle of Incidence, α_o (°)	Percentage of occurrence (%)	Wave Period, T (s)	C_o (m/s)	H_b (m)	d_b (m)	K_{rbr}	α_{br} (°)	V (m/s)	S (m³/year)
	0-1	0.5		0.03	3.96	6.17	0.52	0.63	0.730	20.84	0.89	34
	1-2	1.5		1.45	6.39	9.97	1.46	1.77	0.731	21.66	1.55	26.224
S-SW	2-3	2.5	66	0.36	7.45	11.63	2.36	2.88	0.733	23.85	2.12	23.056
	3-4	3.5		0.00	8.30	12.95	3.22	3.93	0.735	24.72	0.00	0
	4-5	4.5		0.00	9.51	14.84	4.14	5.05	0.728	19.35	0.00	0
	0-1	0.5		0.03	3.96	6.17	0.52	0.63	0.832	15.70	0.70	34
	1-2	1.5		1.31	6.39	9.97	1.46	1.77	0.833	16.30	1.21	24.176
SW	2-3	2.5	44	0.36	7.45	11.63	2.36	2.88	0.835	17.19	1.68	23.627
	3-4	3.5		0.00	8.30	12.95	3.22	3.93	0.836	18.54	0.00	0
	4-5	4.5		0.00	9.51	14.84	4.14	5.05	0.831	14.59	0.00	0
	0-1	0.5		0.14	3.96	6.17	0.52	0.63	0.885	8.02	0.37	103
	1-2	1.5		4.55	6.39	9.97	1.46	1.77	0.886	8.32	0.65	54.427
W-SW	2-3	2.5	21	1.62	7.45	11.63	2.36	2.88	0.886	9.13	0.90	63.599
	3-4	3.5		0.00	8.30	12.95	3.22	3.93	0.886	9.44	0.00	0
	4-5	4.5		0.00	9.51	14.84	4.14	5.05	0.885	7.47	0.00	0
	0-1	0.5		0.33	3.96	6.17	0.52	0.63	0.900	0.39	0.02	13
	1-2	1.5		26.30	6.39	9.97	1.46	1.77	0.900	0.40	0.03	14.825
W	2-3	2.5	1	2.82	7.45	11.63	2.36	2.88	0.900	0.44	0.04	5.634
	3-4	3.5		0.11	8.30	12.95	3.22	3.93	0.900	0.46	0.05	504
	4-5	4.5		0.03	9.51	14.84	4.14	5.05	0.900	0.36	0.05	189
	0-1	0.5		0.56	3.96	6.17	0.52	0.63	0.883	8.75	0.40	444
	1-2	1.5		18.93	6.39	9.97	1.46	1.77	0.883	9.08	0.70	227.058
W-NW	2-3	2.5	23	1.48	7.45	11.63	2.36	2.88	0.883	9.96	0.98	62.807
	3-4	3.5		0.00	8.30	12.95	3.22	3.93	0.884	10.30	0.00	0
	4-5	4.5		0.03	9.51	14.84	4.14	5.05	0.882	8.15	1.06	4.025
	0-1	0.5		0.42	3.96	6.17	0.52	0.63	0.825	16.27	0.72	520
	1-2	1.5		7.86	6.39	9.97	1.46	1.77	0.826	16.89	1.25	147.301
NW	2-3	2.5	46	0.81	7.45	11.63	2.36	2.88	0.828	18.56	1.73	53.501
	3-4	3.5		0.00	8.30	12.95	3.22	3.93	0.829	19.22	0.00	0
	4-5	4.5		0.03	9.51	14.84	4.14	5.05	0.824	15.12	1.91	6.307
	0-1	0.5		0.11	3.96	6.17	0.52	0.63	0.717	21.17	0.91	131
	1-2	1.5		3.07	6.39	9.97	1.46	1.77	0.718	22.00	1.57	54.194
N-NW	2-3	2.5	68	0.53	7.45	11.63	2.36	2.88	0.720	24.23	2.14	32.905
	3-4	3.5		0.06	8.30	12.95	3.22	3.93	0.722	25.11	2.57	7.789
	4-5	4.5		0.00	9.51	14.84	4.14	5.05	0.715	19.65	0.00	0

Table 7. Total Longshore Sediment Transport at Cell 1

Direction of Wave Incoming	Wave Height, H (m)	Sediment Transport (m^3/year)	Total Sediment Transport (m^3/year)	Direction of Sediment Transport
S-SW	0.5	34	49.314	South
	1.5	26.224		
	2.5	23.056		
	3.5	0		
	4.5	0		
SW	0.5	24.176	47.837	
	1.5	23.627		
	2.5	0		
	3.5	0		
	4.5	103		
W-SW	0.5	54.427	114.128	
	1.5	63.599		
	2.5	0		
	3.5	0		
	4.5			
Σ Sediment			211.2	South
W	0.5	13	21.164	North
	1.5	14.825		
	2.5	5.634		
	3.5	504		
	4.5	189		
W-NW	0.5	444	294.334	
	1.5	227.058		
	2.5	62.807		
	3.5	0		
	4.5	4.025		
NW	0.5	520	207.630	
	1.5	147.301		
	2.5	53.501		
	3.5	0		
	4.5	6.307		
N-NW	0.5	131	95.019	
	1.5	54.194		
	2.5	32.905		
	3.5	7.789		
	4.5	0		
Σ Sediment			618.147	North
Net Transport			406.869	North

3.3. Shoreline Change Predictions

The following calculation is to calculate the change in coastline (Δy). The following is an example of calculating coastline changes using the Empiric Method in cell 1:

$$\Delta y = \frac{\Delta t}{d_b \times \Delta x}(Q_{i+1} - Q_i)$$

$$\Delta y = \frac{1}{1{,}77 \times 525{,}68}(219.73 - 406.89)$$

Δy = -0.20 m

The analysis of coastline changes across 15 designated cells (refer to Table 8) indicates distinct spatial patterns of erosion (abrasion) and accretion, influenced by sediment transport processes and hydrodynamic conditions. Over the course of one year (Δt = 1 year), the net sediment transport rate (Qs) and changes in coastline position (Δy) reveal a complex relationship between sediment supply and coastal morphology. Erosion was observed in Cells 1, 2, 4, 7, 10, 14, and 15, with Δy values ranging from -0.02 m (Cell 12) to -0.82 m (Cell 4), indicating a predominant sediment loss. Notably, Cell 4 recorded the most significant erosion rate (Δy = -0.82 m), which corresponds with a high Qs of 461.21 m³/year, likely attributed to its exposure to northward sediment transport (see Tables 6 and 7) and moderate wave energy conditions (H = 1.5–2.5 m; refer to Table 4). In contrast, Cells 3, 5, 6, 8, 9, 13, and 15 experienced accretion, with Δy values ranging from +0.09 m to +0.68 m, where Cell 3 achieved the highest sediment gain (Δy = +0.68 m) despite a low Qs of 10.44 m³/year, suggesting localized sediment deposition due to reduced transport capacity or sheltered environments. The overall direction of net sediment transport (northward, 406,869 m³/year; see Table 7) corresponds with the observed accretion in northern cells (e.g., Cells 3, 5, 6) and erosion in southern cells (e.g., Cells 1, 2), highlighting the effects of littoral drift asymmetry. The consistent Db value (1.77 m) across the cells indicates a uniform nearshore bathymetric profile. In comparison, the variations in Ax (ranging from 148.73 to 1,194.39 m) emphasize the influence of coastline geometry on sediment redistribution. This spatial variability in Δy illustrates the combined effects of wave climate (predominantly from the southwest; see Table 4), sediment grain size (D50: 0.17–0.65 mm; refer to Table 3), and anthropogenic and natural barriers that affect sediment availability.

Table 8. Cell 1 Coastline Changes

Cell	Δx (m)	Δt (tahun)	Db (m)	Q_s (m^3/tahun)	Δy (m)	Ket
1	525.68	1	1.77	406.89	-0.20	Abrasion
2	1136.26	1	1.77	219.728	-0.10	Abrasion
3	375.85	1	1.77	10.44	0.68	Accretion
4	312.32	1	1.77	461.21	-0.82	Abrasion
5	461.54	1	1.77	10.44	0.09	Accretion
6	260.81	1	1.77	87.30	0.45	Accretion
7	241.13	1	1.77	295.37	-0.58	Abrasion
8	155.68	1	1.77	48.90	0.62	Accretion
9	277.19	1	1.77	219.73	0.00	Accretion
10	148.73	1	1.77	219.73	-0.44	Abrasion
11	720.09	1	1.77	104.99	-0.04	Abrasion
12	644.64	1	1.77	48.90	-0.02	Abrasion
13	1194.39	1	1.77	28.06	0.10	Accretion
14	572.31	1	1.77	239.44	-0.19	Abrasion
15	291.41	1	1.77	48.90	-0.09	Abrasion

The graph depicting coastline changes for Cell 1, Figure 10, was created using the CERC methodology [8], demonstrates significant morphological transformations over a ten-year period, highlighting the interaction between sediment transport dynamics and hydrodynamic forces. The data indicates annual variations (Δy) that fluctuate between +10.00 m (indicating accretion) and -10.00 m (indicating erosion), culminating in a net erosion of -0.20 m by the conclusion of the study. This finding is consistent with the sediment budget in Table 8, which shows that Cell 1 experiences a net northward sediment transport of 406,869 m³/year yet still faces erosion due to localized sediment shortages. The annual variability in Δy emphasizes the impact of seasonal changes in wave climate, particularly the prevalence of south-westerly waves (as noted in Table 4) and moderate-energy wave-breaking conditions (as detailed in Table 5), which periodically exacerbate erosion. The negative trend of -0.20 m in the graph is associated with a high capacity for northward sediment transport (as shown in Table 7), indicating that sediment movement from southern cells (such as Cells 1, 2, and 4) to northern accretion areas (like Cells 3, 5, and 6) exceeds the local sediment supply. This situation underscores the significant influence of littoral drift asymmetry and grain size (D50: 0.17–0.65 mm; Table 3) on coastal resilience. The ongoing erosional trend in Cell 1, despite the overall regional patterns of accretion, highlights the necessity for targeted management strategies to rectify sediment imbalances and reduce coastal vulnerability.

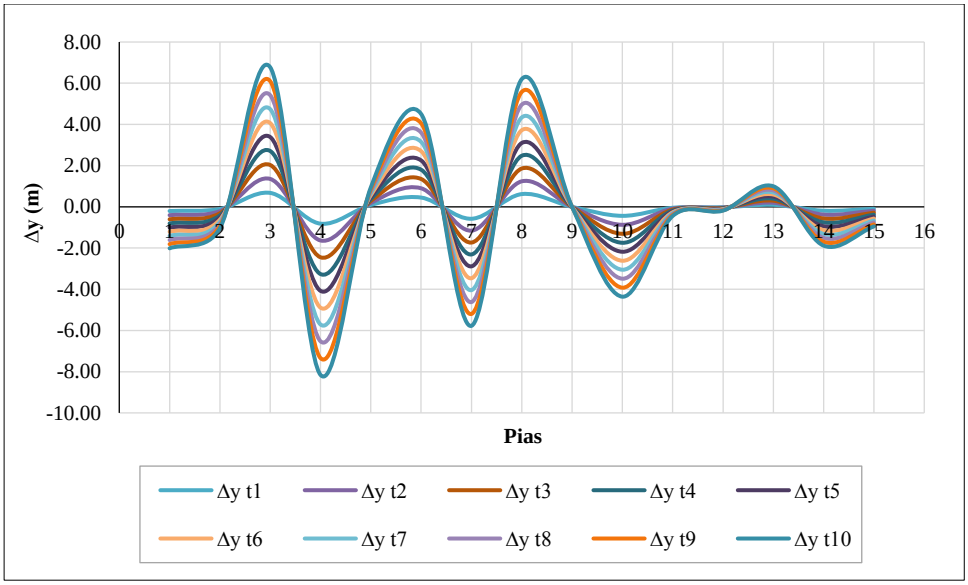

Figure 10. CERC Method Coastline Change Graph

The analysis of shoreline changes presented in Figure 11 to Figure 17, based on numerical modeling utilizing the CERC [8] equations illustrate the spatial variability of coastal dynamics resulting from longshore sediment transport. The fourth channel, with an annual sediment transport rate of 461.21 m³/year, displayed the most significant accretion (-44.85 m), indicative of localized sediment deposition shaped by gradients in wave-driven transport. In contrast, adjacent cells exhibited erosional patterns, emphasizing the diverse responses of coastal areas to hydrodynamic forces. The mapped shoreline alterations from 2014 to 2024 indicate zones of both accretion and retreat, with sediment redistribution influenced by the prevailing wave direction (predominantly south-westerly) and grain size (D50: 0.17–0.65 mm). By combining sediment transport calculations with geospatial mapping (WGS 1984 UTM Zone 51S), this study offers detailed insights into morphological changes, highlighting the effectiveness of numerical models in quantifying shifts in the coastline. This methodology facilitates accurately identifying vulnerable areas, serving as an essential resource for adaptive coastal management strategies.

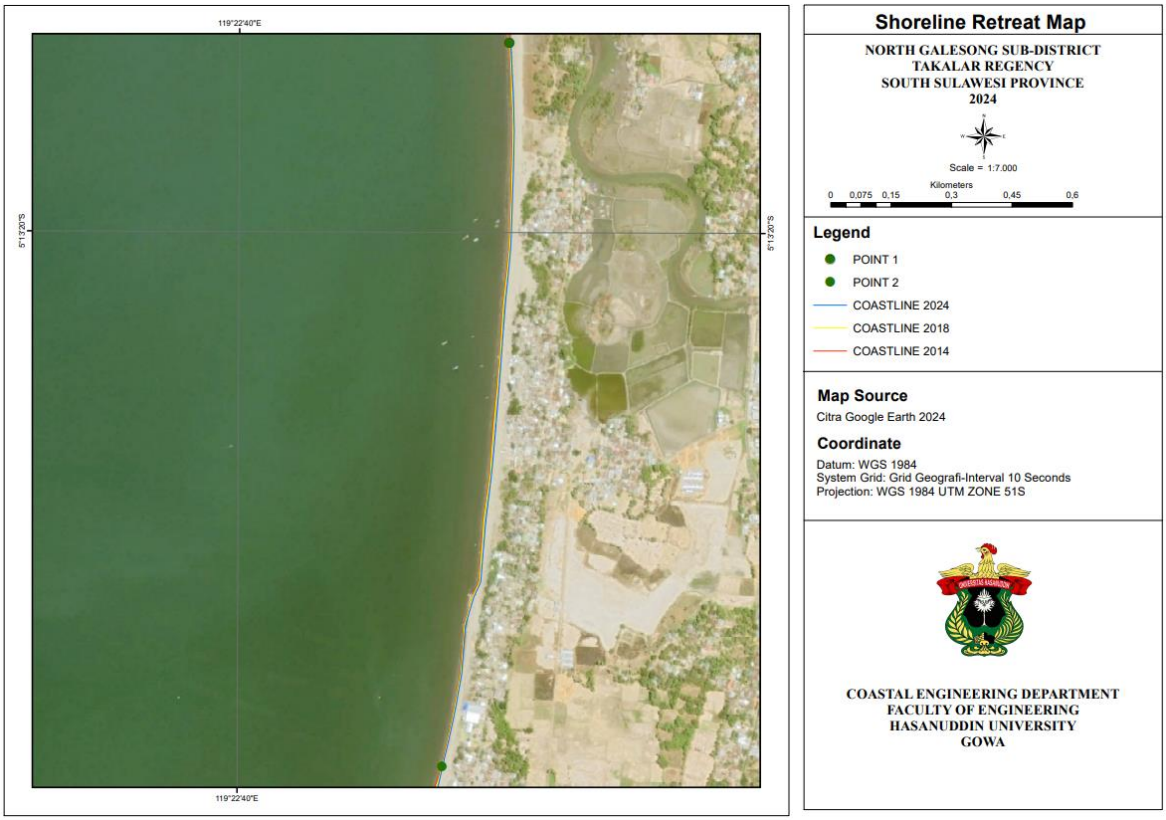

Figure 11. Shoreline changes point 1 and 2

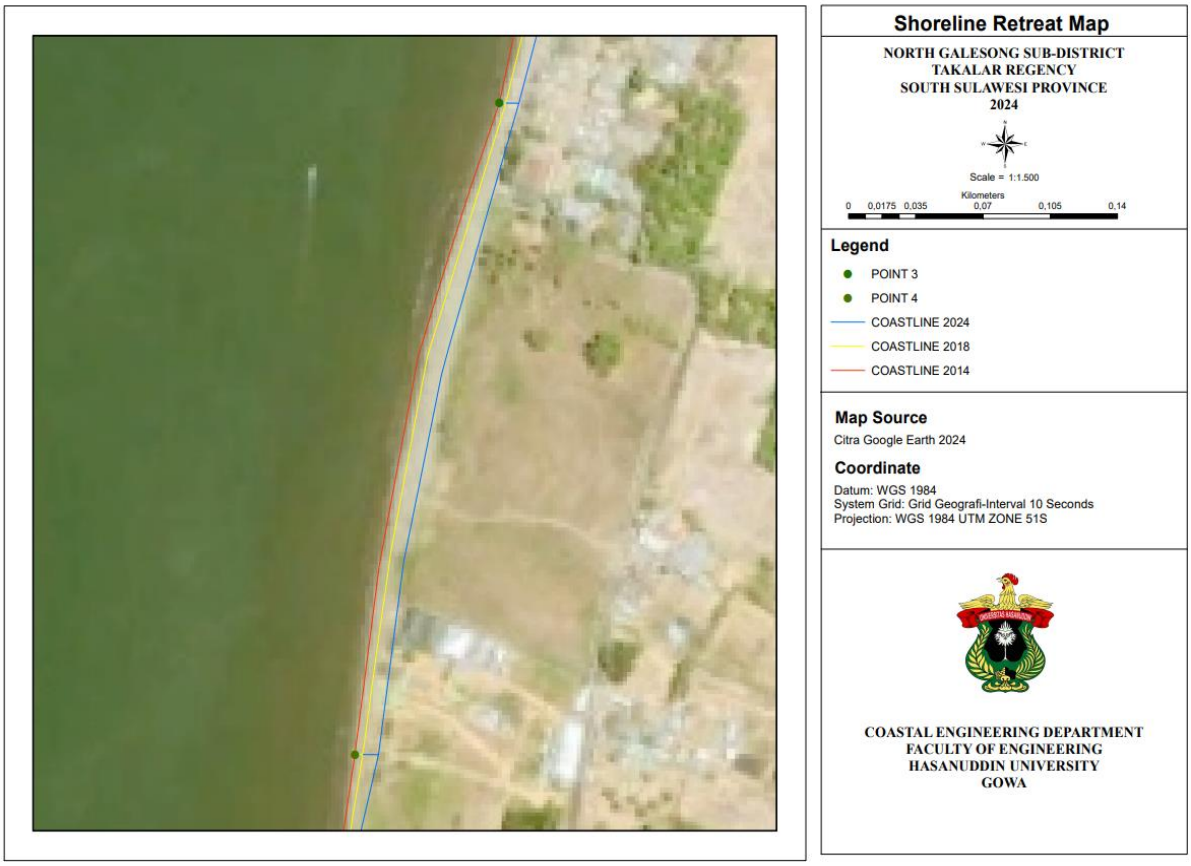

Figure 12. Shoreline changes point 3 and 4

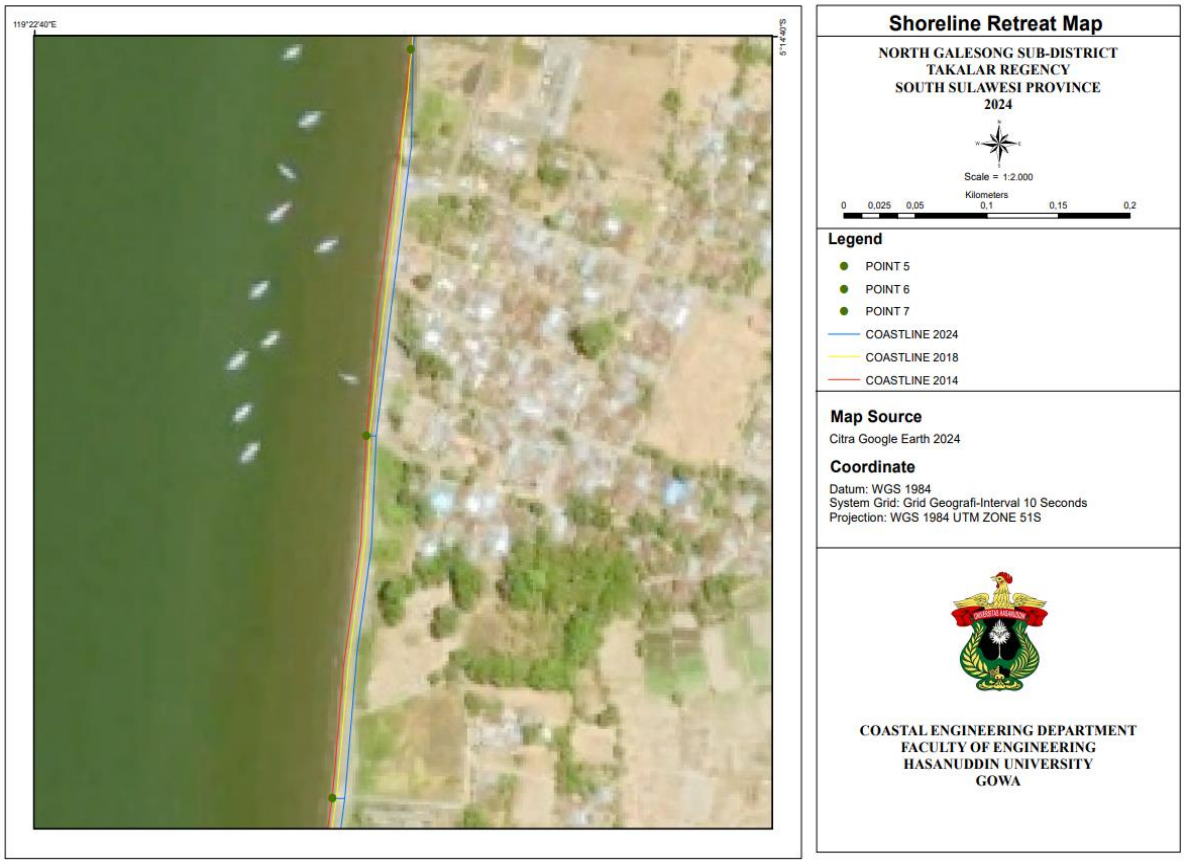

Figure 13. Shoreline changes point 5, 6 and 7

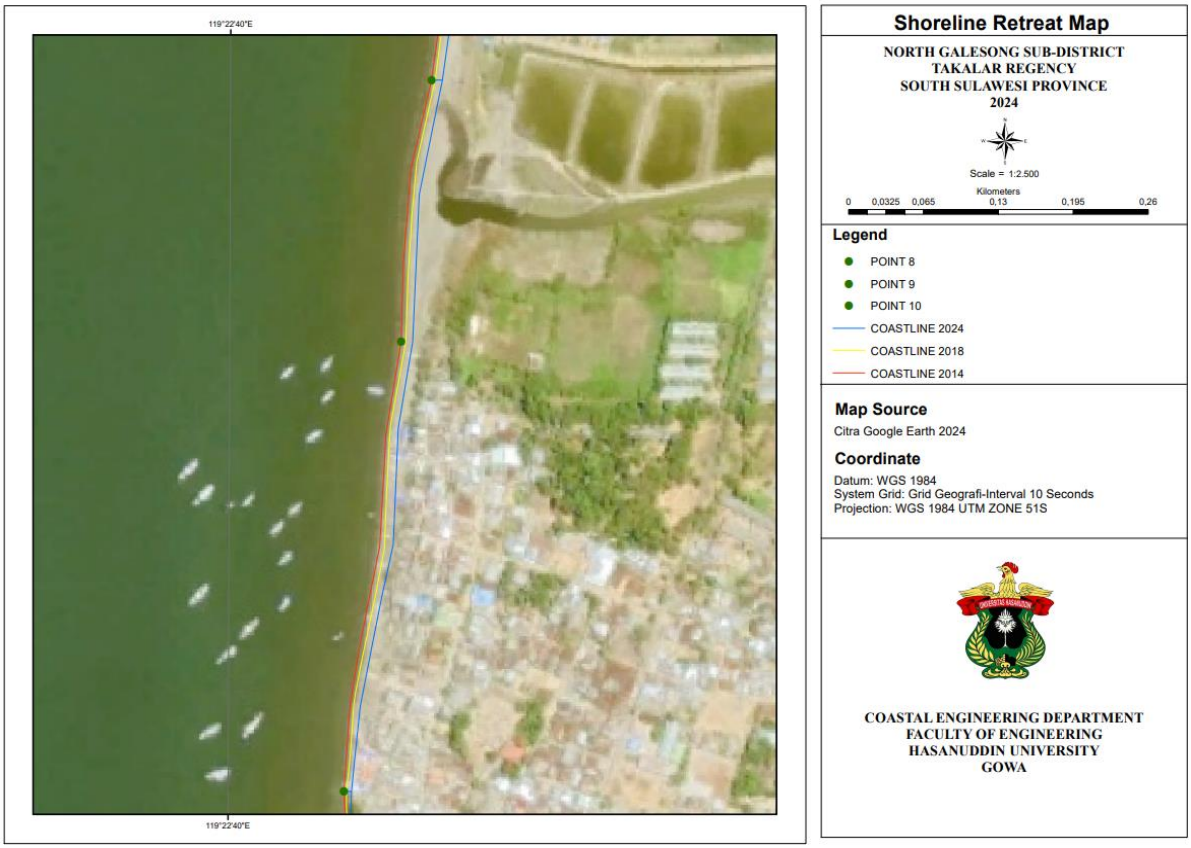

Figure 14. Shoreline changes point 8, 9 and 10

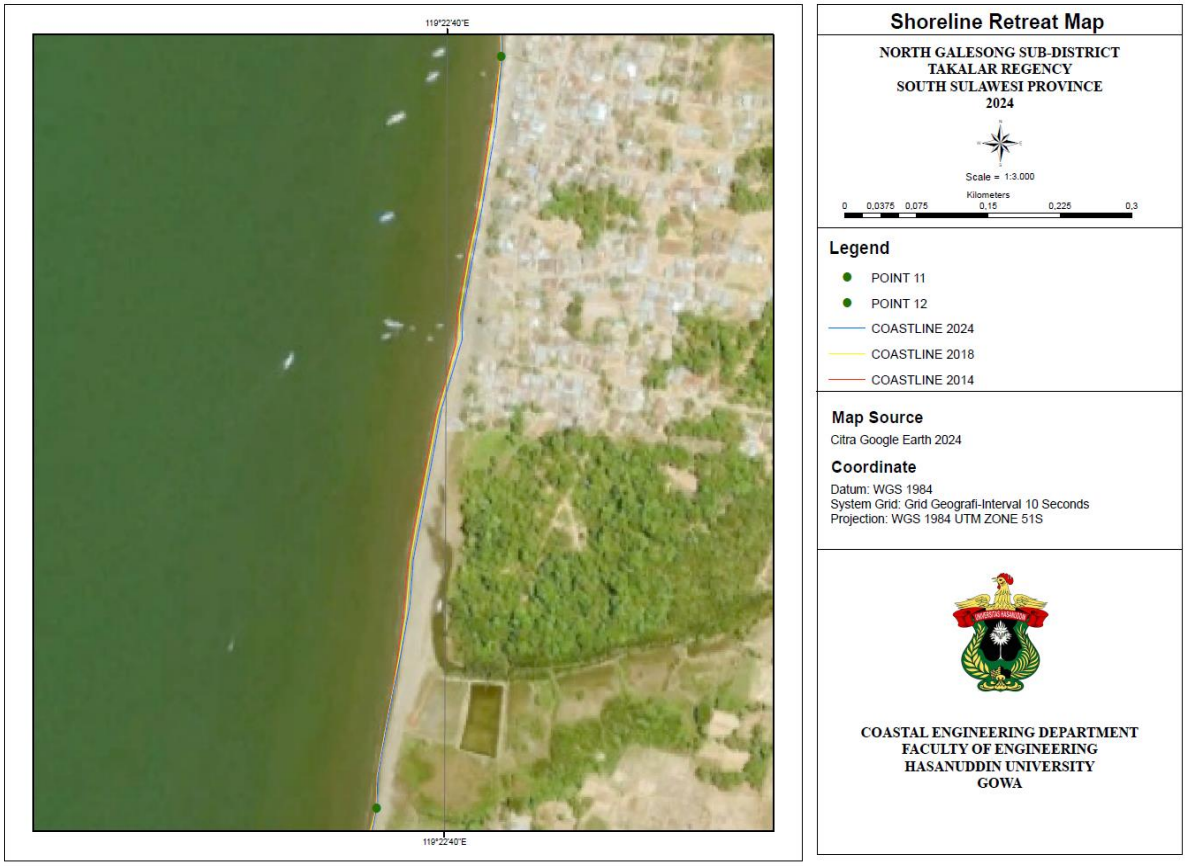

Figure 15. Shoreline changes point 11 and 12

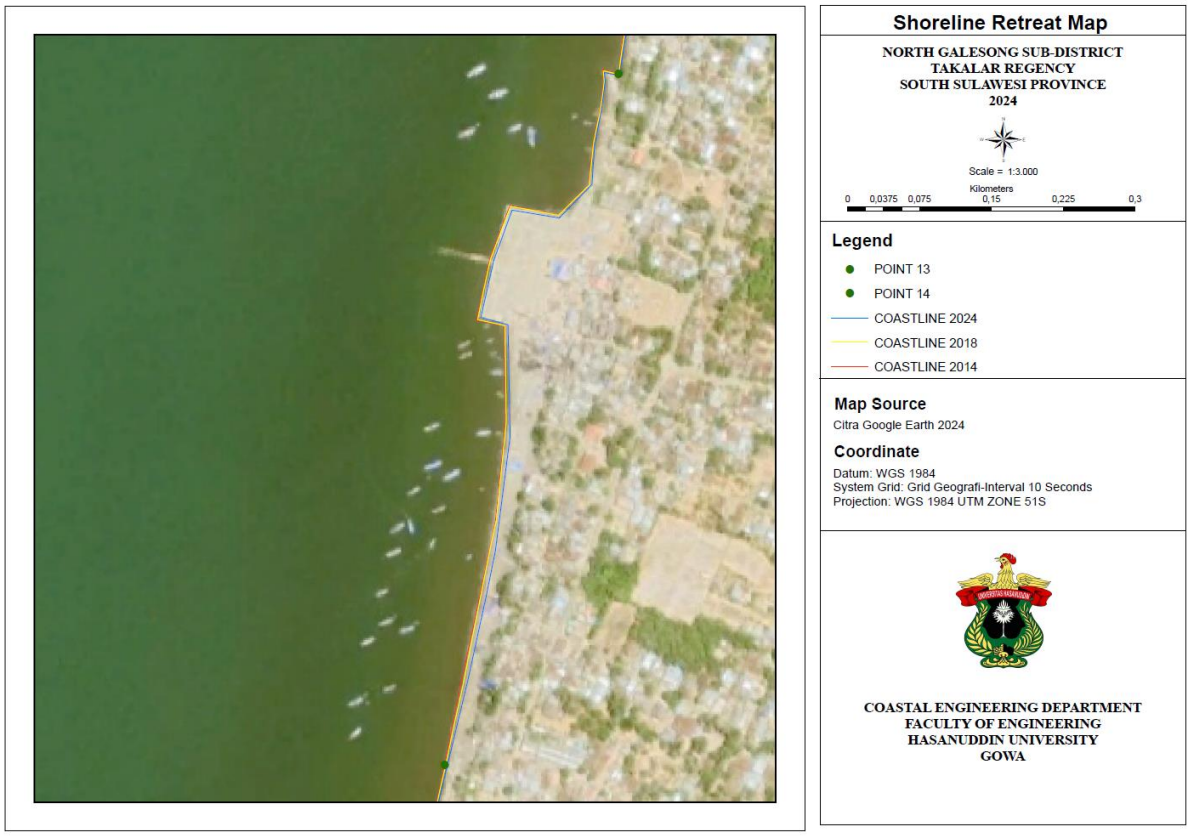

Figure 16. Shoreline changes point 13 and 14

Figure 17. Shoreline changes point 14 and 15

3.4. Spatial Variability Comparisons

The numerical simulation of shoreline dynamics, Figure 18, integrates empirical and numerical modeling to predict coastal changes in the PPI Beba region. Using the finite difference method, it analyzed wave propagation and sediment

transport by incorporating bathymetric data, wave characteristics (height, period, direction), and sediment grain properties. Predictions of shoreline changes, validated against numerical simulations (Fathan, 2024), showed a strong correlation, with deviations within the 20% error margin established by Margotila (2018). This consistency underscores the effectiveness of both methodologies in capturing accretion and erosion patterns, particularly in areas influenced by wave direction (mainly SW-W-NW) and sediment grain size variability (D50: 0.17–0.65 mm). The calibration of the spatial domain, supported by field-validated bathymetric data and shoreline orientation, facilitated accurate modeling of wave distribution, while sediment transport equations enabled predictions of morphological changes under varying hydrodynamic conditions. The combination of empirical and numerical approaches highlights their complementary strengths: empirical models offer rapid, cost-effective assessments of longshore drift, while numerical simulations provide detailed spatiotemporal analyses of wave-sediment interactions.

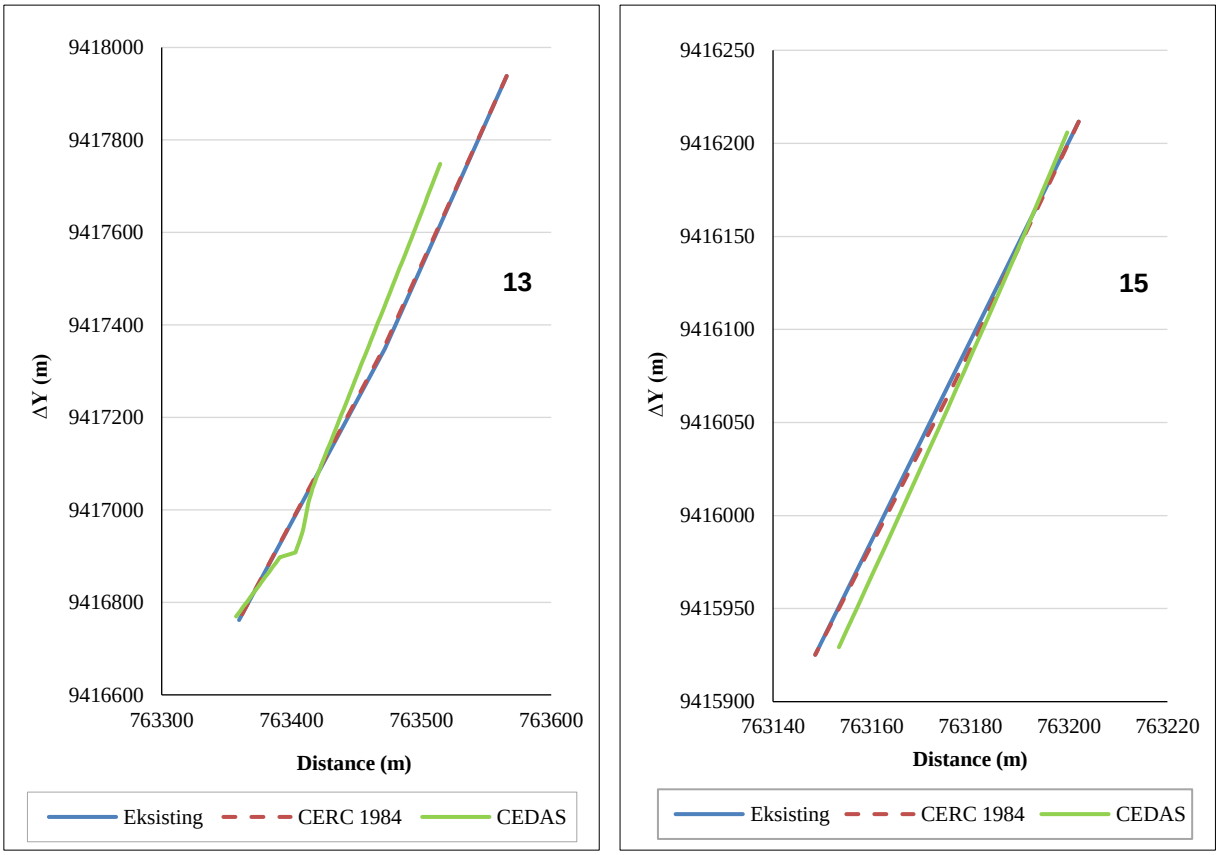

Figure 18. Comparison of Spatial Shoreline changes in selected points

4. Conclusion

This research validates empirical longshore sediment transport (LST) formulas using localized data on waves, sediment, and bathymetry, while forecasting shoreline changes over a decade to identify erosion and accretion zones. The findings reveal that empirical LST models, when tailored with site-specific factors (such as wave direction and sediment grain size D50 between 0.17 and 0.65 mm), align closely with numerical simulations, exhibiting an error margin under 20%. Predictions indicate significant spatial variability in shoreline changes: Cells 1, 4, and 7 experienced notable erosion (Δy: -0.82 m to -0.58 m) due to dominant northward sediment transport (406,869 m^3/year), while Cells 3, 6, and 8 showed accretion (Δy: +0.68 m to +0.62 m) linked to reduced transport capacity and sheltered conditions. The integration of wave climate data (predominantly southwesterly), sediment characteristics, and numerical modeling underscores the critical role of hydrodynamic-sediment interactions in shaping coastal morphology.

This study enhances coastal engineering by demonstrating the efficacy of hybrid empirical-numerical approaches for accurate predictions of sediment transport and shoreline changes, particularly in data-scarce regions. It highlights the importance of localized calibration to address sediment variability and wave asymmetry, offering practical recommendations for erosion management and sustainable shoreline practices. Future research should explore the impacts of long-term climate variability on LST dynamics and validate these models across diverse geomorphic contexts to enhance their global applicability. The results stress balancing empirical efficiency with numerical precision to address coastal vulnerabilities in rapidly changing environments.

5. Declarations

5.1. Author Contributions

Conceptualization, H.U. and C.P.; methodology, T.R., M.R.A., and N.M.; validation, H.U., C.P., and S.H.N.; formal analysis, H.U.; investigation, H.U.; resources, H.U.; data curation, H.U.; writing—original draft preparation, H.U.; writing—review and editing, M.R.A.; visualization, F.M.A. and H.U.; supervision, A.H.M. and M.I.M.; project administration, N.M.; funding acquisition, H.U. All authors have read and agreed to the published version of the manuscript.

5.2. Data Availability Statement

The data presented in this study are available on request from the corresponding author.

5.3. Funding and Acknowledgments

The author would like to thank the Hasanuddin University Research and Community Service Institute (LP2M Universitas Hasanuddin) for providing Collaborative Fundamental Research (PFK) Grant funds with contract number No.00309/UN4.22/PT.01.03/2024 so that the author can conduct this research.

5.4. Conflicts of Interest

The authors declare no conflict of interest.

6. References

[1] Sui, L., Wang, J., Yang, X., & Wang, Z. (2020). Spatial-temporal characteristics of coastline changes in Indonesia from 1990 to 2018. Sustainability (Switzerland), 12(8), 1–28. doi:10.3390/SU12083242.

[2] Schernewski, G. (2016). Integrated Coastal Zone Management. In Encyclopedia of Earth Sciences Series. Springer, Heidelberg, Germany. doi:10.1007/978-94-007-6238-1_183.

[3] Ibrahim, A. S. A., El-Molla, A. M., & Ahmed, H. G. I. (2024). Impacts of Coastal Structures on Sediment Transport: A Case Study of Damietta, Egypt. Nase More, 71(2), 45–53. doi:10.17818/NM/2024/2.1.

[4] Xie, D., Hughes, Z., FitzGerald, D., Tas, S., Asik, T. Z., & Fagherazzi, S. (2024). Longshore Sediment Transport Across a Tombolo Determined by Two Adjacent Circulation Cells. Journal of Geophysical Research: Earth Surface, 129(10), 1. doi:10.1029/2024JF007709.

[5] Firdaus, F., Chaerul, M., & Gusty, S. (2022). Analysis of vulnerability level of beach abration disaster in the District of North Galesong, Takalar Regency. Astonjadro, 11(3), 576. doi:10.32832/astonjadro.v11i3.7195.

[6] Noujas, V., Kankara, R., Raju Alluri, S. K., & Murthy, M. V. R. (2024). Longshore Sediment Transport Rate for Different Energy Regime Coast along the East Coast of India. Journal of Coastal Research, 113(sp1), 110–114,. doi:10.2112/jcr-si113-022.1.

[7] Wang, C., Yang, G., Li, C., Zhao, C., Zhu, J., & Ma, X. (2024). The response of sediment transport and morphological evolution to storms with different characteristics. Science of the Total Environment, 946(173987), 1. doi:10.1016/j.scitotenv.2024.173987.

[8] CERC. (1984). Shore Protection Manual. US Army Corps of Engineers, Coastal Engineering Research Center, Washington United States.

[9] Komar, P. D., & Inman, D. L. (1970). Longshore sand transport on beaches. Journal of Geophysical Research, 75(30), 5914–5927. doi:10.1029/jc075i030p05914.

[10] Pananrangi, A. I. (2015). Land Utilization in Galesong Coastal Area Based on Abrasion Disaster Risk Analysis. Plano Madani: Jurnal Perencanaan Wilayah Dan Kota, 4(2), 22–31. (In Indonesian).

[11] Prasetyo, A. F., Rachman, T., & Paotonan, C. (2020). Identification of Coastal Damage in the Coastal Area of North Galesong District, Takalar Regency, South Sulawesi. Riset Sains Dan Teknologi Kelautan, 3(1), 26–31. doi:10.62012/sensistek.v3i1.13236. (In Indonesian).

[12] Zhiddiq, S., Rauf, B., Yusuf, M., Maddatuang, M., & Mannan, A. (2023). Geospatial Information on Abrasion Disaster Risk in South Sulawesi. LaGeografia, 21(3), 321. doi:10.35580/lageografia.v21i3.51200. (In Indonesian).

[13] Hastuti, A. W., Ismail, N. P., & Nagai, M. (2023). Coastline change detection using high-resolution satellite images: A case study in Amurang Coasts, South Minahasa, North Sulawesi. IOP Conference Series: Earth and Environmental Science, 1251(1), 012011. doi:10.1088/1755-1315/1251/1/012011.

[14] Rahmawati, R. R., & Lee, J. L. (2023). Beach Erosion Assessment According to Maritime Mining and its Excavation Condition According to Erosion Tolerance Standards. SSRN (Preprint), 1-24. doi:10.2139/ssrn.4594311.

[15] Theocharidis, C., Doukanari, M., Kalogirou, E., Christofi, D., Mettas, C., Kontoes, C., Hadjimitsis, D., Argyriou, A. V., & Eliades, M. (2024). Coastal Vulnerability Index (CVI) Assessment: Evaluating Risks Associated with Human-Made Activities along the Limassol Coastline, Cyprus. Remote Sensing, 16(19), 1–22. doi:10.3390/rs16193688.

[16] Coca-Domínguez, O., & Ricaurte-Villota, C. (2019). Validation of the Hazard and Vulnerability Analysis of Coastal Erosion in the Caribbean and Pacific Coast of Colombia. Journal of Marine Science and Engineering, 7(8), 260. doi:10.3390/jmse7080260.

[17] Cao, X., Sun, Y., Wang, Y., Wang, Y., Cheng, X., Zhang, W., Zong, J. K., & Wang, R. (2024). Coastal erosion and flooding risk assessment based on grid scale: A case study of six coastal metropolitan areas. Science of the Total Environment, 946(174393), 1. doi:10.1016/j.scitotenv.2024.174393.

[18] Badwi, N., Baharuddin, I. I., & Abbas, I. (2019). Abrasion Hazard Mitigation Efforts on The Coast Maros Regency of South Sulawesi, Indonesia. Proceedings of the 1st International Conference on Advanced Multidisciplinary Research (ICAMR 2018), 104. doi:10.2991/icamr-18.2019.104.

[19] Ningsih, N. S., Azhari, A., & Al-Khan, T. M. (2023). Wave climate characteristics and effects of tropical cyclones on high wave occurrences in Indonesian waters: Strengthening sea transportation safety management. Ocean & Coastal Management, 243. doi:10.1016/j.ocecoaman.2023.106738.

[20] Senior, N., Matthews, A., Webber, B., Latos, B., & Baranowski, D. (2023). Extreme precipitation in South Sulawesi triggered by equatorial waves and its representation in MetUM forecasts. Tropical Meteorology and Tropical Cyclones, EGU23-6549, doi:10.5194/egusphere-egu23-6549.

[21] Haiyqal, S. V., Ismanto, A., Indrayanti, E., & Andrianto, R. (2023). Characteristics of Sea Wave Height during Normal, El Niño and La Niña Periods in the Makassar Strait. Jurnal Kelautan Tropis, 26(1), 190–202. doi:10.14710/jkt.v26i1.17003.

[22] Badan Pusat Statistik. (2021). Takalar Regency in Figures. Badan Pusat Statistik, Kabupaten Takalar, Indonesia. (In Indonesian).

[23] Triatmodjo, B. (1999). Coastal Engineering. Beta Offset, Yogyakarta, Indonesia. (In Indonesian).

[24] Fuad, M. A. Z., Yunita, N., Kasitowati, R. D., Hidayati, N., & Sartimbul, A. (2019). Long-Term Shoreline Change Monitoring Using Geo-Spatial Technology on the West Coast of Tuban Regency, East Java. Jurnal Geografi, 11(1), 48–61. doi:10.24114/jg.v11i1.11409. (In Indonesian).

[25] Raihansyah, T., Setiawan, I., & Rizwan, T. (2016). Study of Coastline Changes in the Coastal Area of Ujung Blang Waters, Banda Sakti District, Lhokseumawe. Jurnal Ilmiah Mahasiswa Kelautan Dan Perikanan Unsyiah, 1(1), 46–54. (In Indonesian).

[26] Hegde, A. V., & Akshaya, B. J. (2015). Shoreline Transformation Study of Karnataka Coast: Geospatial Approach. Aquatic Procedia, 4, 151–156. doi:10.1016/j.aqpro.2015.02.021.

[27] Putra, I. G. F., & Santosa, B. (2023). Analysis of Shoreline Changes Using Empirical Methods at Palik Beach, North Bengkulu. Jurnal Teknik Sipil, 19(2), 246–264. doi:10.28932/jts.v19i2.5953.